The new CMCC Seasonal Prediction System SPS4

Technical Notes
June 2025
Issue TN0301

CLIVAP – Climate Variability and Prediction

*By **Antonella Sanna***
Fondazione CMCC Centro Euro-Mediterraneo sui Cambiamenti Climatici
antonella.sanna@cmcc.it, silvio.gualdi@cmcc.it, marianna.benassi@cmcc.it, andrea.borrelli@cmcc.it, daniele.peano@cmcc.it, mehri.hashemidevin@cmcc.it, andrea.cipollone@cmcc.it, stefano.tibaldi@cmcc.it

=== Acknowledgments ====
The research leading to these results has received funding from C3S2_370 contract and has been carried out with the computational support of CINECA.

SUMMARY The present Technical Note outlines the new CMCC Seasonal Forecast System CMCC-SPS4 which will replace in operations, from August 1st, 2025, the current system version CMCC-SPS3.5. The System is based on the new CMCC Ocean-Atmosphere Global Climate Model, developed and implemented at CMCC, the CMCC-CM3, which will be the basis for a large variety of activities, going from seasonal and decadal predictions to climate projections, in an almost seamless framework. The system performances are documented both in a "climate" perspective, that is running the system in climatological mode, with present-climate forcings and climatological initial conditions, and in seasonal forecast mode, with realistic initialization and temporal horizon of 6 months.

Keywords GCM, Earth System Model, QBO, Seasonal Forecasts, Ensemble Forecasts

1. INTRODUCTION

The novel version of the CMCC coupled model stems from the Community Earth System (CESM) project (https://www.cesm.ucar.edu/) developed at the National Centre for Atmospheric Research (NCAR) in the United States. In particular, the third version of the CMCC coupled model (CMCC-CM3) derives from the CESM version 2 (CESM2, Danabasoglu et al., 2020). The main differences between CMCC-CM3 and CESM2 resides in the oceanic and river components. In particular, the CMCC-CM3 uses the Nucleus for European Modelling of the Ocean (NEMO) as ocean component, since CMCC is part of the NEMO consortium (https://www.nemo-ocean.eu/) and it is involved in its development, while the river routing module, HYDROS (Materia et al. in preparation), has been developed at CMCC, stemming from the RTM model. Figures 1 and 2 illustrate the general schemes of the two, old and new, CMCC-CM2 and CMCC-CM3 fully coupled Earth System Models.

The report is organized as follows: after a brief description of the model components (Section 3), the main characteristics of the performance of CMCC-CM3 will be presented by means of a 30-year-long simulation, using constant present-day (2000) climate forcing (Section 4). The model performance will be evaluated against observations and re-analysis data and against a similar simulation, carried out with the previous version of the model, CMCC-CM2, specifically developed at the time to be the basis for the currently operational Seasonal Forecasts System CMCC-SPS3.5. The last part of the report (Section 5) is specifically devoted to some very preliminary results of the CMCC-SPS4, the new Seasonal Prediction System. In this last part, results will be presented in terms of ensembles with a reduced number of hindcast members for the two canonical start-dates of November and May (focusing on lead season one forecasts, namely DJF

and JJA respectively) and will be illustrated in terms of biases, anomaly correlation coefficients and teleconnection indices. Section 6 summarizes the conclusions and Section 7 is devoted to the references.

This is the list of the acronyms used in the report:

CMCC-CM3 refers to the new global circulation model developed at CMCC

CMCC-CM2 is the old version currently operational

CMCC-SPS3.5 is the Seasonal Prediction System currently operational

CMCC-SPS4 is the new upcoming SPS

CMCC-SPS3.5-CLIM refers to a present climate simulation carried out with the climatological version of CMCC-SPS3.5

CMCC-SPS4-CLIM refers to a present climate simulation carried out with the CMCC-CM3

TREFHT refers to 2m-temperature

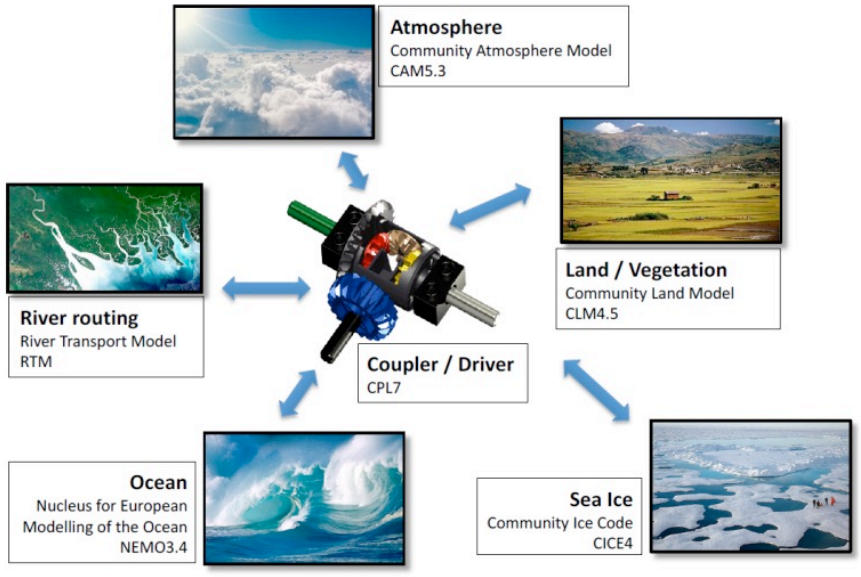

Figure 1. General scheme of the CMCC-CM2 fully coupled Global Model

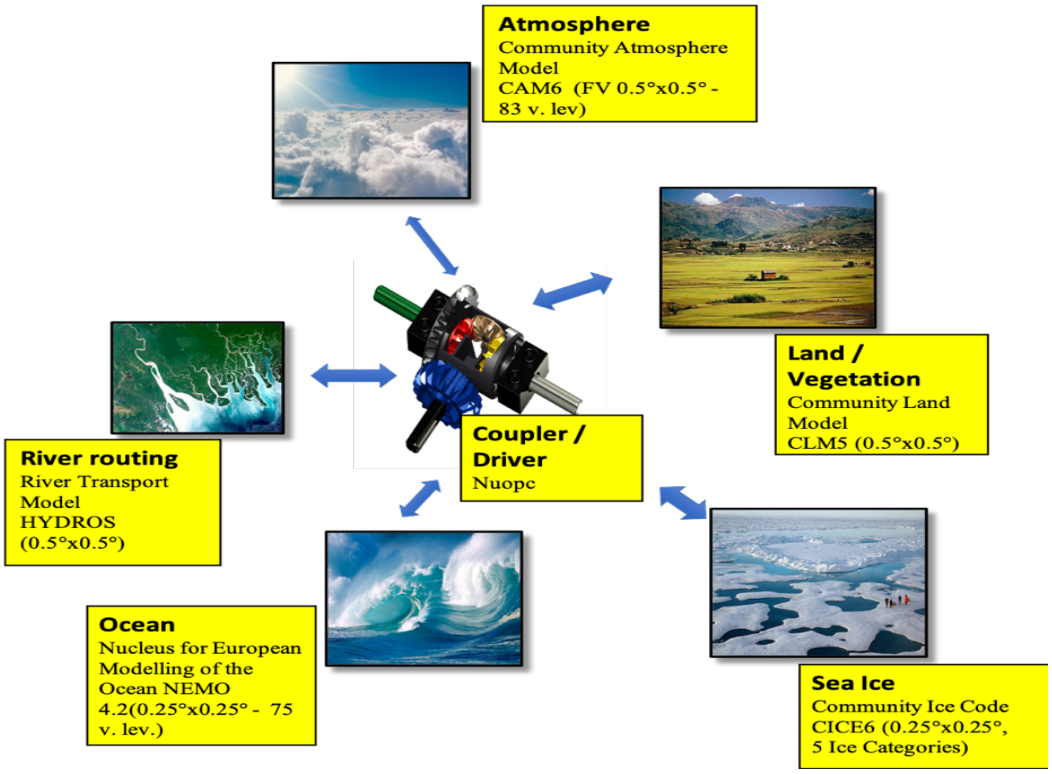

Figure 2. General scheme of the CMCC-CM3 fully coupled Global Model

2. DESCRIPTION OF THE NEW CMCC-CM3

2.1. ATMOSPHERE

The atmospheric component of CMCC-CM3 is the Community Atmosphere Model Version 6 (CAM6, Craig et al., 2021), with Finite Volume (FV) dynamical core (Lin and Rood, 1997). It replaces the former CAM5.3, which makes use of a Spectral Element dynamical core.

The sixth version of CAM, compared to the fifth version which was implemented in CMCC-CM2 (Cherchi et al., 2019), presents changes in all parameterizations but for radiation, which is still based on the Rapid Radiative Transfer Model for General circulation models (RRTMG; Iacono et al., 2008). In particular, CAM6, compared to previous versions, contains: i) the unified turbulence scheme, Cloud Layers Unified By Binormals (CLUBB; Golaz et al., 2002; Larson, 2017), which uses a multivariate binormal probability density function describing sub-grid scale variations in temperature, humidity, and vertical velocity; ii) an updated version of the Morrison-Gettelman cloud microphysics scheme (MG2; Gettelman & Morrison, 2015); iii) the Modal Aerosol Model version 4 (MAM4; Liu et al., 2016) to represent aerosols; iv) a new sub-grid orographic form drag parameterization (Beljaars et al., 2004); v) an anisotropic orographic gravity wave drag scheme following Scinocca and Mcfarlane (2000). Further details can be found in Danabasoglu et al. (2020) and Craig et al. (2021).

In CMCC-CM3, CAM6 is implemented with a regular grid of 0.47° × 0.63° (therefore at a horizontal resolution of about 0.5°) and a vertical resolution consisting of 83 vertical hybrid levels, covering Troposphere and Stratosphere up to 0.01 hPa approximately. In the presently operational version, an equivalent horizontal resolution is implemented, yet with a coarser vertical resolution (46 instead of 83 vertical levels, less refined in the

Stratosphere). The latter improvement in the new system is expected to allow a more realistic representation of Stratosphere dynamics and its related feedbacks on the Troposphere.

2.2. OCEAN

The Nucleus for European Modelling of the Ocean model in its version 4.2 (NEMO4.2, Madec et al., 2022) is the ocean components of the novel CMCC Coupled Model (CMCC-CM3). The physical engine of NEMO resolves the classic primitive equations of ocean circulation subject to the Boussinesq, hydrostatic and incompressibility approximations. The prognostic variables are the three velocity components, the sea surface height, the potential temperature, and salinity. With respect to the NEMO3.4, implemented in CMCC-SPS3.5, NEMO4.2 improved i) the bulk formula for air-sea interaction (Brodeau et al., 2017); ii) the representation of tracker advection; iii) the treatment of vorticity by means of two new energy conserving scheme; iv) the domain configuration in case of north-south and east-west periodicity. Further details may be found in Madec et al. (2022).

NEMO4.2 is run with a tripolar ORCA grid based on Mercator projection (Madec & Imbard, 1996), with a horizontal resolution of about 0.25° (as it is in the present operational model) and 75 levels (with a finer vertical resolution with respect to the currently operational 50 ones) in the vertical.

2.3. SEA-ICE

The sea-ice component of CMCC-CM3 is based on the Los Alamos Sea Ice Model version 6 (CICE6, Hunke et al., 2018 and CICE consortium github https://github.com/CICE-Consortium/CICE). It replaces the previously operational CICE4, run so far with a single

sea-ice category, to be compliant with the presently operational ocean analysis, produced with LIM, as sea-ice module.

CICE6 is released with Icepack version 1.1, which is available as a stand-alone package (https://github.com/CICE-Consortium/Icepack.git). A major difference compared to the version used in CMCC-CM2 is represented by the Icepack model, which deals with the column physics, such as the ice thickness distribution. Moreover, different rheology schemes are available in CICE6. The Elastic-Viscous-Plastic (EVP) scheme (Hunke and Dukowicz, 1997) is used in the CMCC-CM3 configuration. The EVP scheme is a modification of the standard Viscous-Plastic model for sea-ice (Hibler, 1979).

CICE6 is run on the same ocean grid and accounts for 5 ice categories (with respect to the single category in CICE4, as mentioned above), 8 ice layers, and 3 snow layers.

2.4. LAND SURFACE

The Community Land Model version 5.1 (CLM5.1) is the land component of the novel CMCC Coupled Model (CMCC-CM3). Compared to version 4.5, which was implemented in CMCC-CM2, CLM5 improves various land parameterizations (Lawrence et al., 2019) such as i) dynamic land units; ii) hydrology and snow structure and parameterization; iii) plant hydraulics; iv) revised nitrogen cycle; v) urban module; vi) stomatal physiology; and vii) crop module. CLM5.1 is used at a horizontal resolution of about 0.5°, with a regular grid of 0.47° × 0.63°, same as the atmospheric module grid. Differently from the default configuration of CLM5.1, the CMCC-CM3 version of CLM5.1 uses the snow density parameterization by Anderson (1976), instead of the version by van Kampenhout et al. (2017), and accounts for a tuning factor to adjust the snow aging, computed using the method by Flanner and Zender (2006). CLM5.1 accounts for 20 soil layers down to 8 meters and 5 additional bedrock layers down to 42 meters.

With respect to the currently operational version, the land surface model is implemented with the biogeochemical component, to allow for the simulation of the biogeochemical cycles. In the current CMCC-SPS3.5 system this module is switched off, because the system is only used to carry out seasonal forecasts. The new CMCC-SPS4 is meant to be one of the applications of a seamless system, which will be used to run a wider range of simulations, going from extended-seasonal to decadal.

2.5. RIVER ROUTING

The HYdro-Dynamic ROuting Scheme (HYDROS) is the river transport scheme used in CMCC-CM3. Differently from the River Transport Model (RTM, Graham et al., 1999), preswntly used in CMCC-CM2, HYDROS uses a more complex scheme in computing the flow velocity. In particular, HYDROS generates time-dependent flow velocity based on a Darcy-Weisbach equation (Darcy, 1857; Weisbach, 1845). Consequently, the flow velocity depends on the orography and the amount of water available in the river. Further details and a comparison between HYDROS and RTM will be found in Materia et al. (2025, in preparation).

HYDROS is run on a 0.5° regular grid and receives the amount of water to route directly from the land surface model, with a 3-hour frequency.

2.6. COUPLER

CMCC-CM3 inherits the CESM2 coupling infrastructure, which is derived from a collaborative effort to create an infrastructure able to build and run the model as well as to control the state and flux exchange between the components. This framework is named Common Infrastructure for Modelling Earth (CIME, https://github.com/CMCC-Foundation/cime). CIME allows modularity in order to facilitate the introduction of new components and models in the coupling infrastructure. CIME provides also a Case

Control System (CCS, https://github.com/CMCC-Foundation/ccs_config_cmcc) used for configuring, compiling, and executing the coupled model on recognized machines. Additional coupling components are used in managing the data configurations (Community Data Models for Earth Prediction System, CDEPS, https://github.com/CMCC-Foundation/CDEPS), which are cases with model components represented by external data forcing, instead of active models, driving and initializing models (National Unified Operational Prediction Capability, NUOPC, part of the Earth System Modelling Framework, ESMF, https://earthsystemmodeling.org/, replacing the currently operational MCT) and customizing coupling code, such as flux calculations and averaging (Community Mediator for Earth Prediction System, CMEPS, https://github.com/CMCC-Foundation/CMEPS).

Land, atmosphere, and sea-ice communicate state and fluxes information through mediator and driver every 30 minutes, while the ocean exchanges information every hour. The transmission of information between land and river module takes place every 3 hours.

3. PRESENT CLIMATE OF THE COUPLED MODEL CORE

The following two Sections are devoted to the evaluation of the performance of CMCC-SPS4 in terms of the climate of its coupled model core (CMCC-CM3, this Section 3) and to some preliminary results of the CMCC-SPS4 in reforecast mode (Section 4). The model performance is evaluated against observations and re-analysis data and against the performance of the previous version of the model, CMCC-CM2 for the climate model core and CMCC-SPS3.5 for the full Seasonal Prediction System.

In the long integration presented in this section, the ocean initial conditions for temperature and salinity are taken from the 2018 World Ocean Atlas (Locarnini et al.,

2018; Zweng et al., 2018) and homogeneous sea-ice concentrations are set for ice coverage typical for boreal winter. The land component is initialized with a two-phase spin-up procedure (Koven et al., 2013; Lawrence et al., 2019): the first phase consists of a 400 year simulation, in which the carbon and nitrogen pools are accelerated to reach an annual turnover timescale, followed by additional 800 years in "normal mode", under pre-industrial forcings. The second phase is a historical run from 1850 to present, in order to reach the correct balance between components and allow for investigation of interannual variability. We recall that the atmospheric forcings are kept constant to a cyclical year 2000, in order to simulate present climate conditions.

3.1. GLOBAL MEAN CLIMATE

In this subsection, we analyze the global mean climate, as simulated by the new CMCC-CM3 in climatological mode, focusing on 2m-Temperature (t2m) and Total Precipitation. Having in mind the use of CMCC-CM3 as basis for CMCC-SPS4 and that of CMCC-CM2 for CMCC-SPS3.5, in the following, we will use the acronyms CMCC-SPS4-CLIM (for CMCC-CM3) and CMCC-SPS3.5-CLIM (for CMCC-CM2) for the two present climate simulations carried out with the two model versions.

The global mean t2m is compared (not shown) with the ERA5 field, averaged over a 20-year period centered on 2000 (1990–2009), which is about 14.24 °C (14.4 °C, over the entire reference period 1993-2022). In the CMCC-SPS4-CLIM model, this value is realistically reproduced (about 14.25 °C). The mean climate is analyzed in terms of the two main seasons, boreal winter (DJF) and boreal summer (JJA). Results are compared with both the CMCC-SPS3.5-CLIM and the observations (ERA5 for t2m and GPCP- Adler et al. 2003- for precipitation; reference period 1993-2022).

The t2m bias with respect to ERA5 re-analyses (1993-2022) is shown in Figure 3, in terms of for the two versions of the CMCC coupled model present climate run (CMCC-

SPS4-CLIM on the left and CMCC-SPS3.5-CLIM on the right): boreal winter results are shown in top panels, while summer ones in the bottom. The most striking feature of the CMCC-SPS3.5-CLIM is the presence of a bias characterized by the same pattern, regardless the season examined: very cold in the Northern hemisphere and mainly hot in the Southern. The new model CMCC-SPS4-CLIM (left panels) presents features that are more seasonally-dependent, such as the warm bias over the summer regions (especially South-America and South-Africa, in Figure 3 top left, and North America, Europe and central Asia, in Figure 3 bottom left) and over Alaska. Globally, the biases are reduced in both of the seasons examined with respect to CMCC-SPS3.5-CLIM.

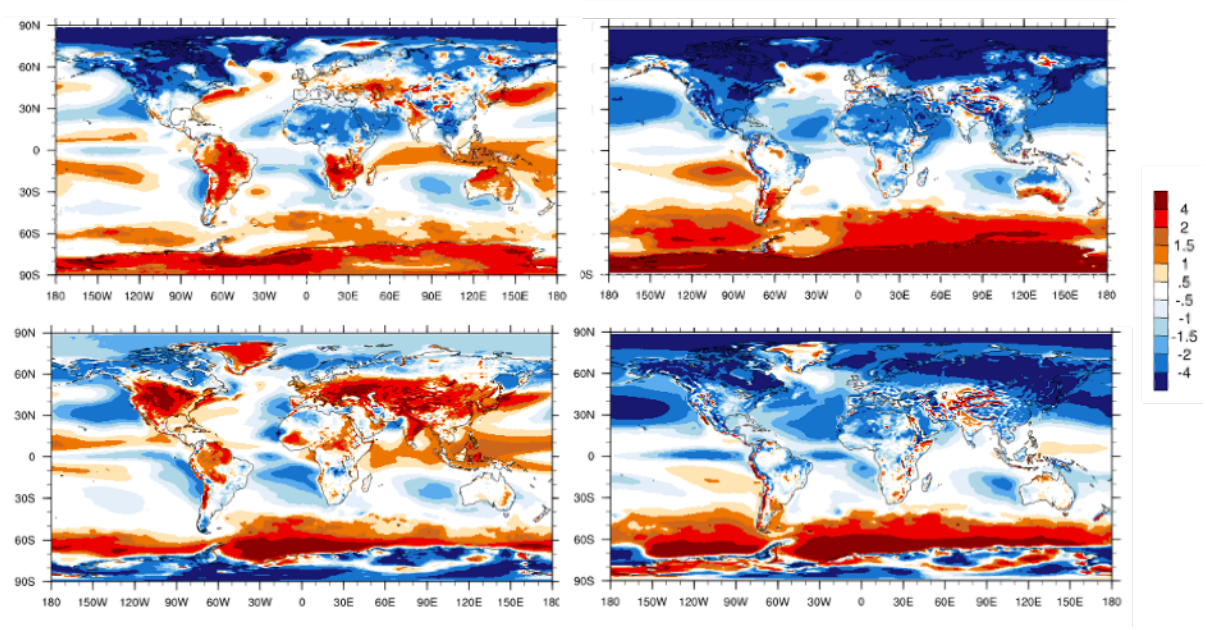

Figure 3. Boreal winter (top) and boreal summer (bottom) t2m bias. Left panels show CMCC-SPS4-CLIM while right ones CMCC-SPS3.5-CLIM (see text above for an acronym list). Biases are computed against ERA5 1993-2022

The annual cycle is compared against the ERA5 climatology and is shown in Figure 4 in terms of the global average. The new CMCC-SPS4-CLIM is represented by the blue curve, while the CMCC-SPS3.5-CLIM by the green one. Observations are in red. The cold bias, characterizing the global annual cycle of the CMCC-SPS3.5-CLIM, is largely reduced in the new model version, thanks to a reduction of the bias, especially in the Northern Hemisphere (not shown). On the contrary, boreal summer months exhibit a slight overestimation.

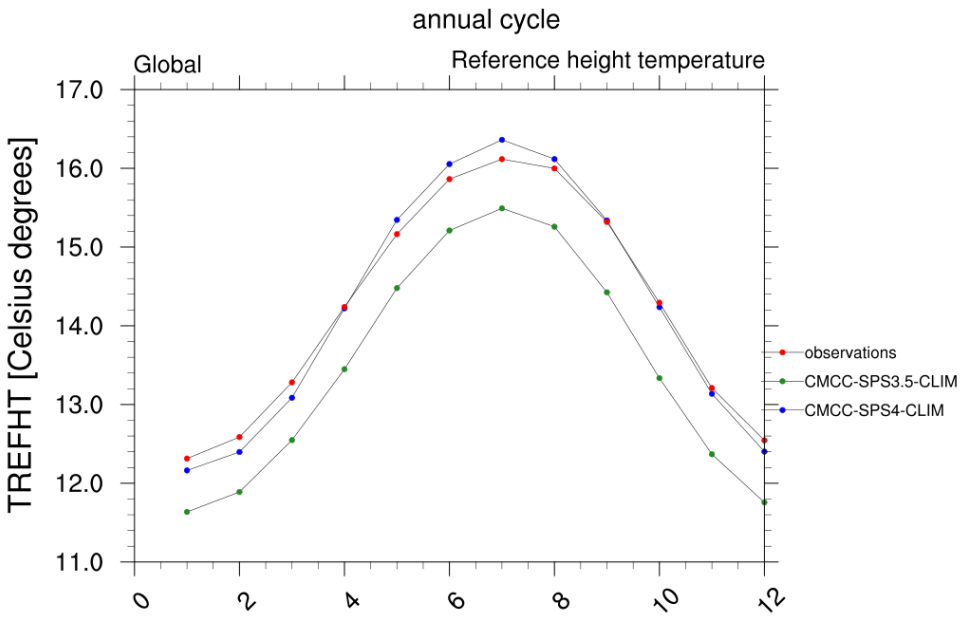

Figure 4. Global annual cycle of t2m (TREFHT in the plot). Blue curve represents the CMCC-SPS4-CLIM, green one the CMCC-SPS3.5-CLIM. Red curve represents the observations -ERA5, 1993-2022. Units are Celsius degrees.

For precipitation, the bias is shown in Figures 5, for boreal winter in the upper panels and summer in the lower ones. Model results are compared against observed GPCP climatology, referring to 1993-2022. The main characteristics of the patterns produced by the model do not change between the two versions: dry biases along the coast of

Alaska, northern Med-Sea, part of Siberia and, the most relevant, the dry area over Amazon basin, which is a well-known weakness of the CAM model (Yin et al, 2012). The biases over ocean are overall reduced in the new model CMCC-SPS4-CLIM (especially over Pacific), but for the Indian Ocean. Boreal summer season (Figure 5 bottom panels) exhibits similar patterns between the two model versions, yet biases are overall stronger in the new model version (bottom left panel), especially over India.

The annual cycles for Total Precipitation are shown in Figure 6. As in Figure 4, the blue curve represents the new CMCC-SPS4-CLIM, the green one the CMCC-SPS3.5-CLIM and the red curve the observations. The large positive bias of the CMCC-SPS3.5-CLIM is strongly reduced, thanks to a reduced overestimate of the precipitation over the Southern Hemisphere (not shown). Nevertheless, the model still tends to overestimate the global mean observed values, especially during boreal summer.

3.2. QBO TUNING

CMCC-CM2 and, therefore, CMCC-SPS3.5 are both unable to capture and reproduce the QBO, which is considered an important phenomenon in the framework of Seasonal Predictions, since it involves time-ranges which are relevant for this category of forecasts.

In order to obtain an internally generated QBO with a reasonable period, the CAM parameter (*eff_beres_dp*), controlling the efficiency of convectively generated gravity waves, has been tuned, changing it from 0.4 to 0.55. The resulting QBO compares reasonably well with observations. For the tuning process devoted to this specific phenomenon, an additional simulation (CMCC-SPS4-CLIM_qbo) was carried out, differing from the CMCC-SPS4-CLIM only for the *eff_beres_dp* parameter (further increased from 0.5 to 0.55). A period of 18-years was considered to be sufficient to

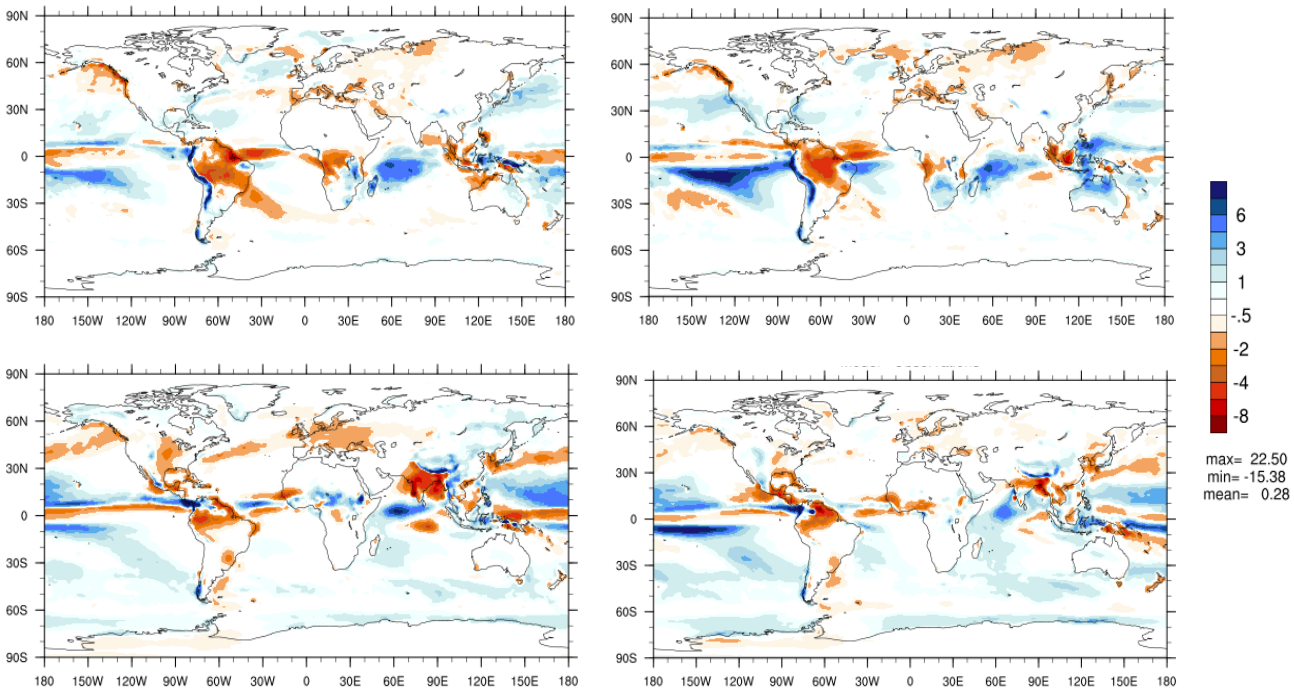

Figure 5. Boreal winter (top) and boreal summer (bottom) Total Precipitation bias. Left panels show CMCC-SPS4-CLIM while right ones CMCC-SPS3.5-CLIM. Biases are computed against GPCP 1993-2022.

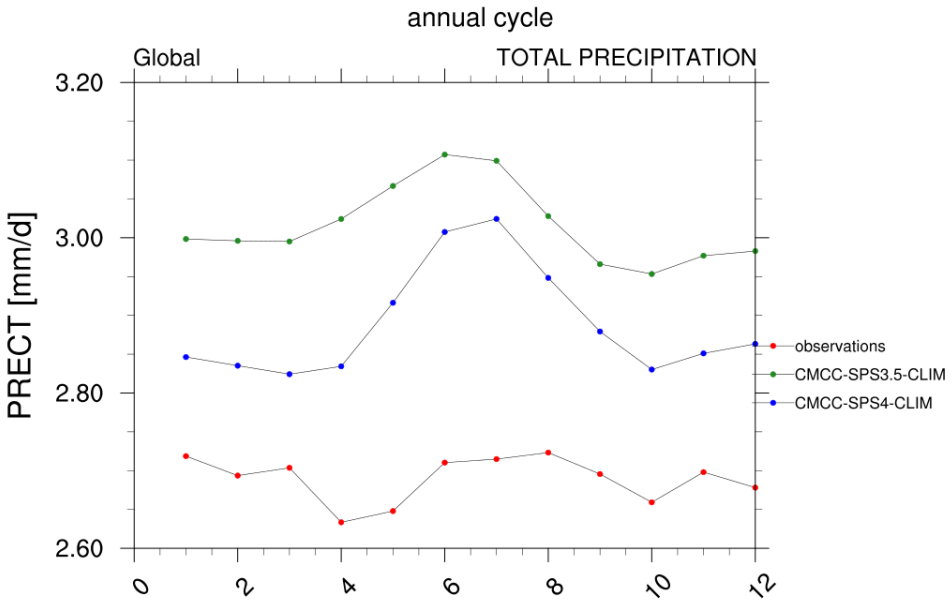

Figure 6. as Figure 4 but for Total Precipitation. Observations provided by GPCP (reference period 1993-2022).

analyze the model behavior in simulating the QBO. Figure 7 illustrates the QBO index (zonal mean zonal wind averaged between -5 and +5 degrees latitude). In order to compare the two simulations with the observations, an arbitrarily selected 18 year-long time-window for CMCC-SPS3.5-CLIM and observations is plotted against the results from CMCC-SPS4-CLIM_qbo. The CMCC-SPS3.5-CLIM is clearly incapable of reproducing the phenomenon; instead, the new model captures fairly well the frequency and the intensity of the observed QBO.

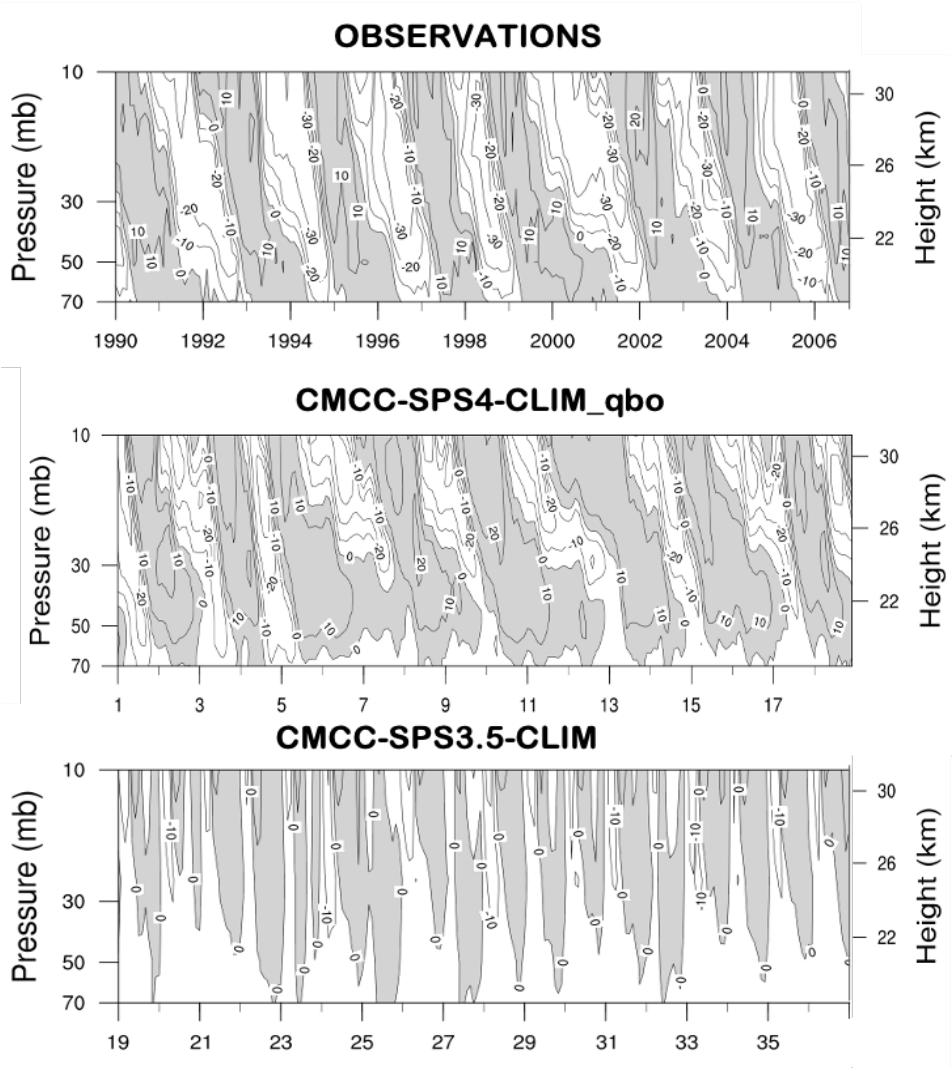

Figure 7. 18-year-timeseries of QBO index (zonal mean zonal wind, averaged in the latitudinal belt 5°S - 5°N). Y axis shows pressure levels in the Stratosphere, from 70 to 10 hPa. The top panel shows the observed QBO (arbitrarily selected 18 years from 1990), the middle one the CMCC-SPS4-CLIM_qbo QBO and bottom the CMCC-SPS3.5-CLIM QBO (arbitrarily selected 18 years from the 30-year-long present climate simulation).

3.3. CLIMATE VARIABILITY INDICES

The following section of the report is devoted to the two most relevant climate variability indices at the NH mid-latitudes, namely NAO and ENSO, analyzed in order to show the CMCC-CM3 model capability, even in the simpler present-climate experimental setup, to generate an internal variability comparable to observations.

To assess the capability of the CMCC-CM3 model to represent the teleconnection patterns associated with the two indices, the composites of precipitation and t2m during their two phases have been computed and contrasted against the observations, taking as reference period that of the CMCC-SPS3.5 hindcasts, namely 1993-2016.

3.3.1. NAO

The NAO index (computed following the definition of Li and Wang 2003) is shown in Figure 8 (black line) for the 30-year integration of CMCC-CM3, together with the corresponding one derived from ERA5, over the reference period 1993-2022 (red curve). The occurrence of the peaks is obviously different in the two curves, because in the present-climate experimental set-up the external forcing is kept constant, so that the variability is purely internally generated, yet the amplitude and the frequency are reasonably well reproduced by the model.

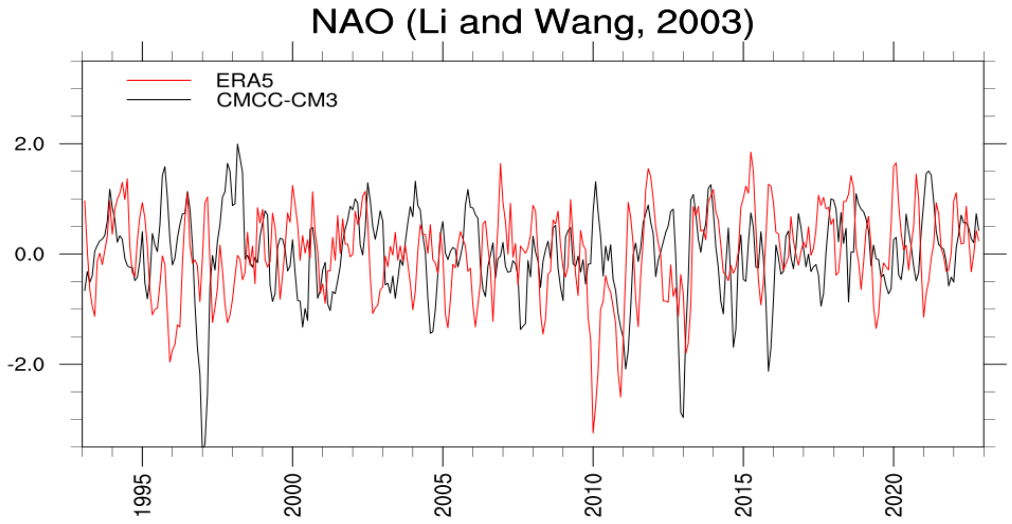

Figure. 8 NAO Li and Wang index monthly timeseries: Observations from 1993 to 2022 (new C3S reference period) are shown in red, against the 30-year CMCC-CM3 model present-climate internally generated NAO in black.

Figure 9 shows the composite patterns of the precipitation field, associated to the positive and the negative phase of the boreal winter (DJF) NAO, with the CMCC-CM3 model results on the left and observations (GPCP) on the right. The positive phase composites are shown in the upper panels, while the negative phase ones in the lower panels. The positive NAO phase is associated with a stronger than usual Atlantic jet stream and a northward shift of the storm track. This results in wetter than normal conditions over the British Isles and drier than normal conditions over the Mediterranean basin. Compared to the observations, the model tends to produce a wider area of wetter than normal conditions around 60N latitude in the positive phase, yet the main features of the teleconnection are correctly captured. Similar considerations apply for the negative phase, shown in the bottom panels.

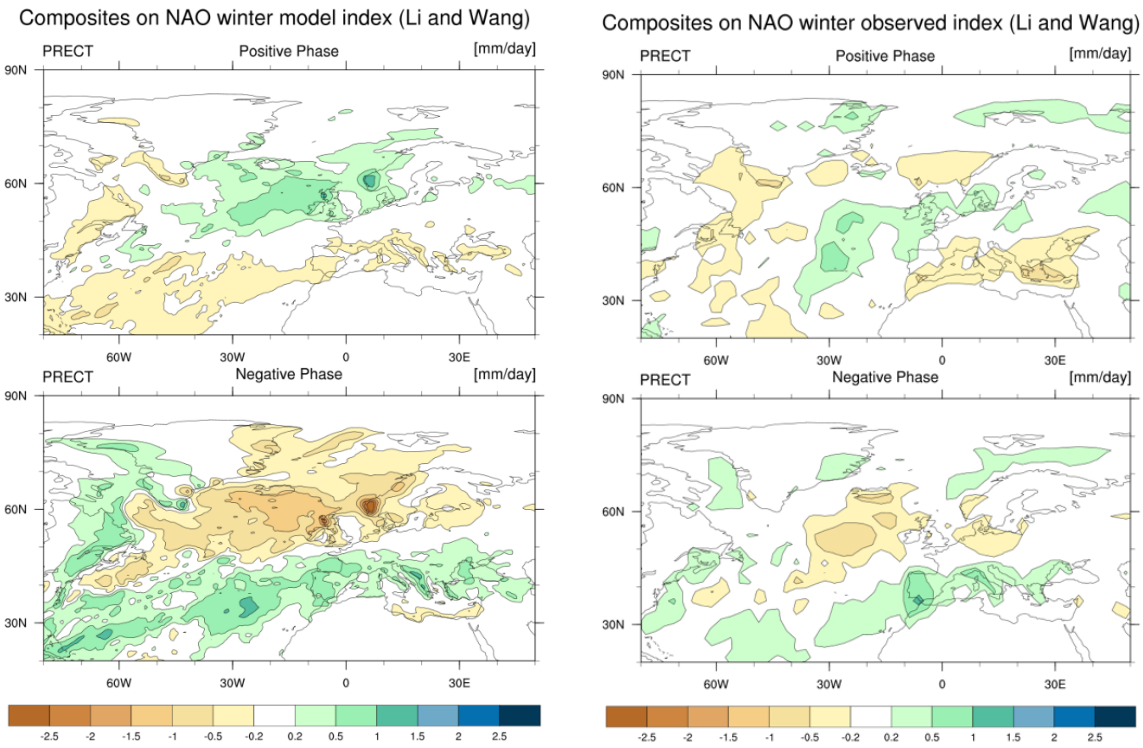

Figure 9. Boreal winter (DJF) Euro-Atlantic patterns of Total Precipitation composited on the NAO index. Upper panels show the positive phase and lower panels negative phase. Left panels CMCC-CM3 model results, right panels observations (GPCP).

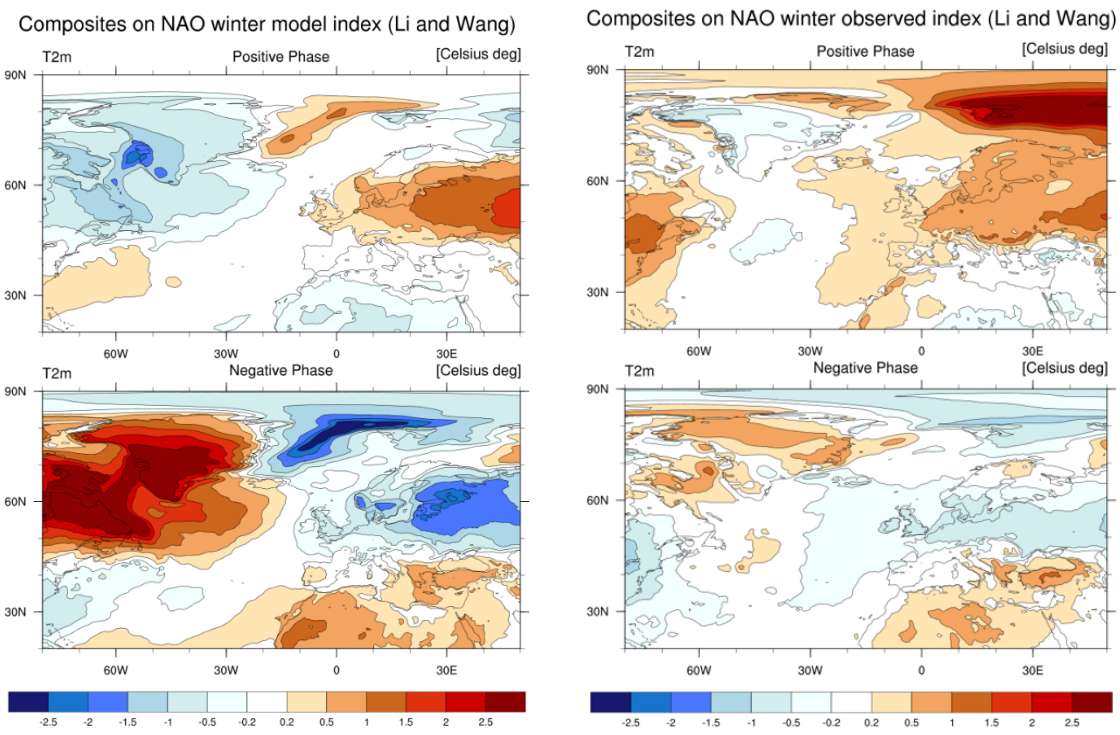

Figure 10 Same as Figure 9, but for t2m. Observations from ERA5.

Figure 10 shows a similar comparison for t2m. As expected from the well-known teleconnection pattern, in the positive phase (top panels), Northern Europe experiences warmer-than-average temperatures, associated with air masses advected from lower latitudes; opposites conditions occur in the negative phase (lower panels). Compared to ERA5, in the positive phase the model tends to confine the European centers of the anomalies on the continental areas, while in the negative phase the anomaly over Europe is more intense, as it is the one over the North Atlantic, off the coast of Greenland. Overall, the main teleconnection features over Europe are correctly reproduced in both phases.

3.3.2. ENSO

The El Nino Southern Oscillation is investigated by means of the Nino3.4 index, computed from the sea surface anomalies (SST) over the Pacific region delimited by 5N-5S, 170W-120W. This index can be thought of as representing the average equatorial SSTs across the central Tropical Pacific.

Figure 11 shows the internally generated Nino3.4 index variability of CMCC-CM3 with the black curve and the observed one (ERA5 re-analyses) with the red one. The curves are not in phase because of the model set-up (constant year 2000 annual forcing), but the amplitude and the frequency of the observed variability are very well captured by the model.

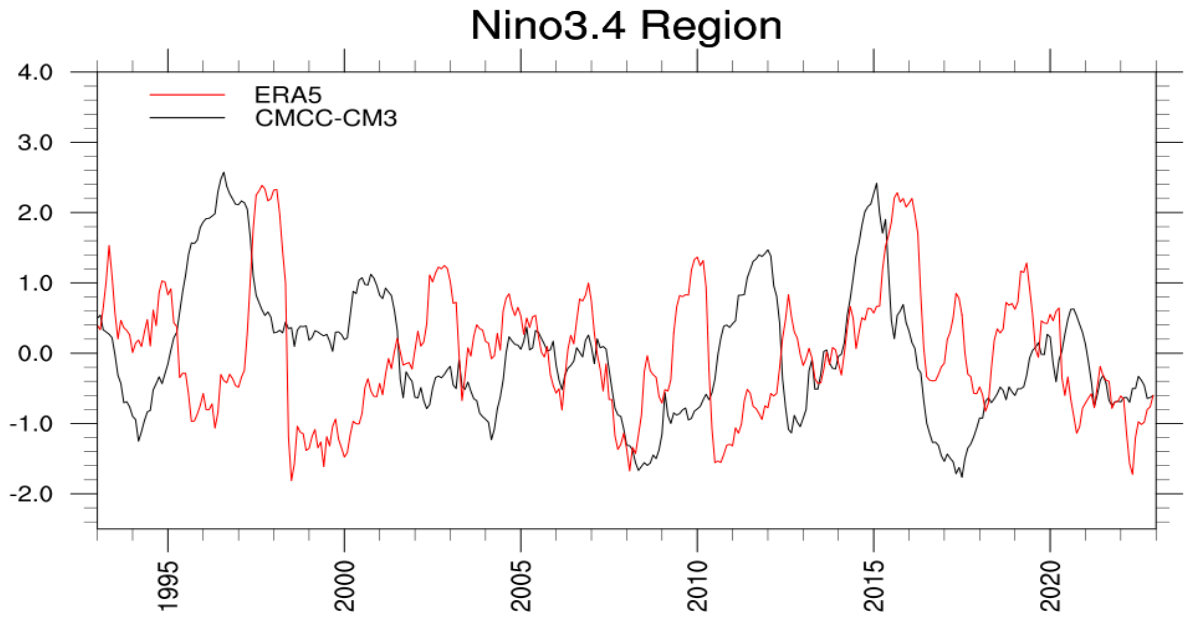

Figure 11. Nino3.4 index monthly timeseries: Observations from 1993 to 2022 are shown in red, CMCC-CM3 in black.

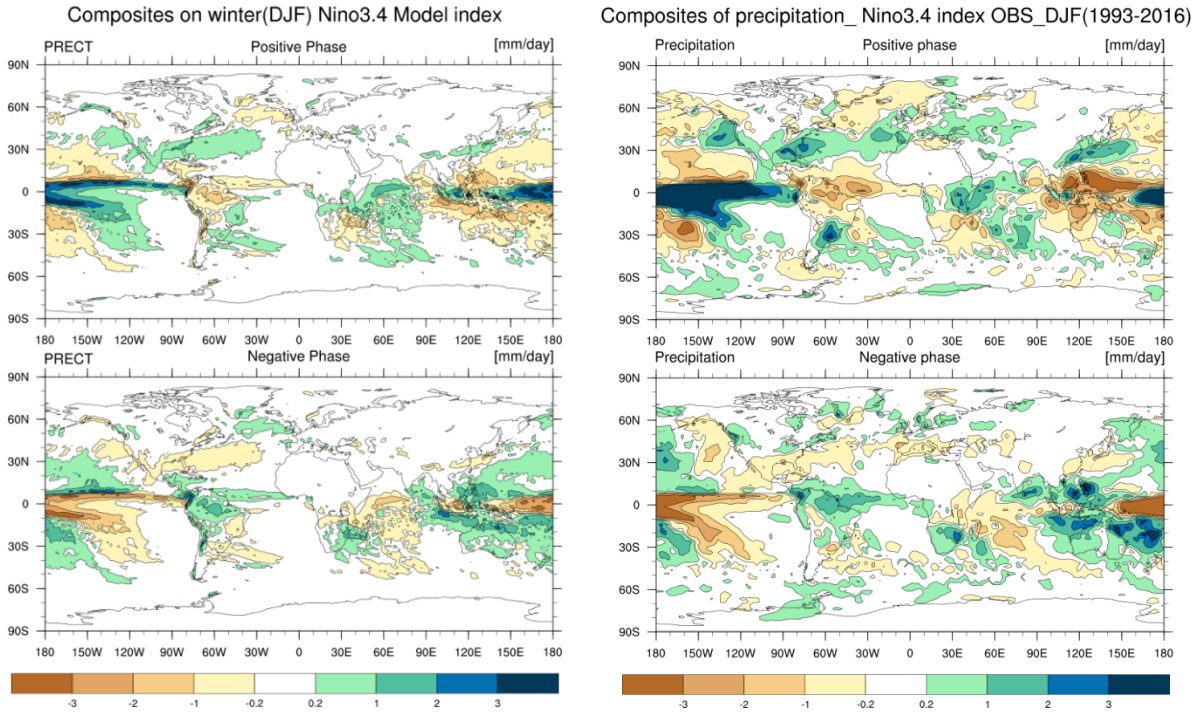

Figure 12. Boreal winter (DJF) global patterns of Total Precipitation composited on the Nino3.4 index. Upper panels show the positive phase while lower panels the negative phase. Left panels CMCC-CM3 model results, right panels observations (GPCP).

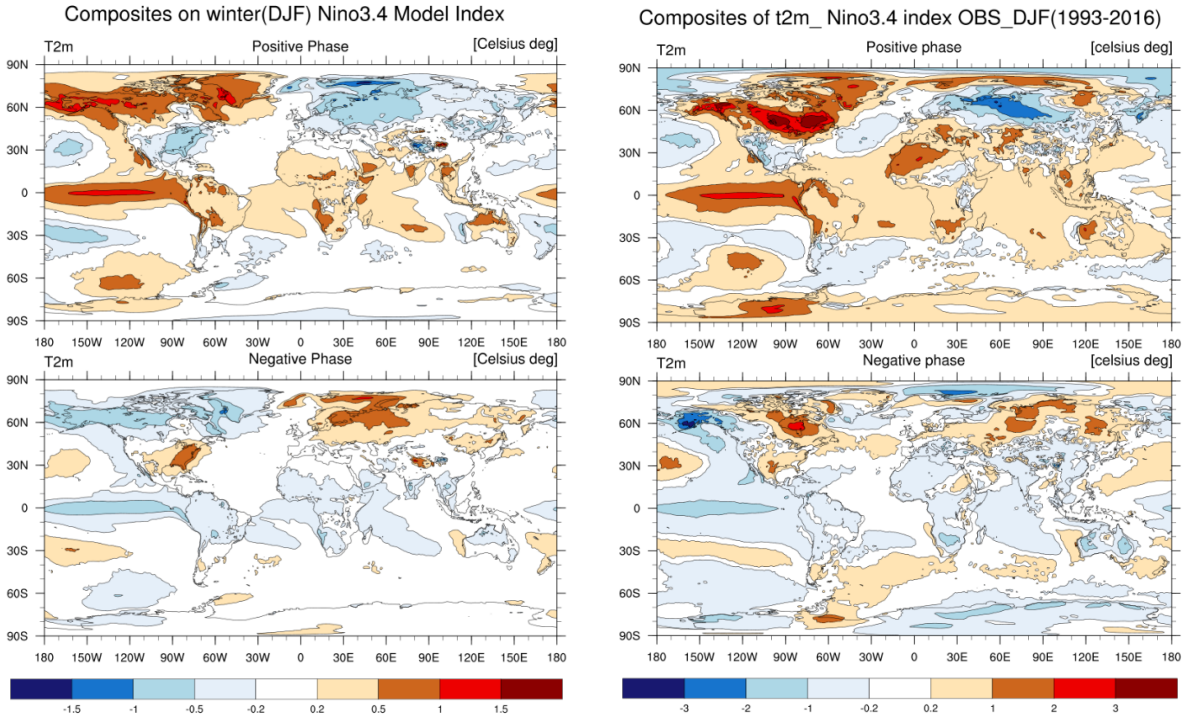

Figure 13. Same as Figure 12, but for t2m. Observations are ERA5.

Similarly to what was done for the NAO, the composite maps of Total Precipitation and t2m are computed for the positive and negative phases of the Nino3.4 index, focusing on boreal winter season (DJF). Results are compared with observations (GPCP and ERA5 respectively) and shown in Figure 12 for precipitation and in Figure 13 for t2m, with upper panels showing the composites relative to the positive phase and lower ones to the negative one.

Focusing on precipitation (Figure 12), the main features of the well-known teleconnection pattern are reasonably well reproduced by the model. The positive phase (upper panels) is characterized by wetter than normal conditions over equatorial Pacific, with suppressed convection over maritime continent and Amazon basin. Drier than normal conditions are correctly simulated over southern Africa and, to some extent, over

Australia. The negative phase (bottom panels) exhibits the suppressed convection over central Equatorial Pacific, well reproduced in the model, as it is the enhanced convection over Brazil and Maritime continent. Conversely, in both phases, the teleconnection patterns over Northern Hemisphere are largely missed or underestimated.

The t2m teleconnection patterns are shown in Figure 13. In the positive phase (top panels) the warm tongue associated with higher than average temperature conditions over the Tropical Pacific is correctly captured by the model, as it is the band of positive anomalies on the northern Pacific along the coast of the US up to the Alaska. Overall, the patterns over the oceans are correctly represented in the model. Over the continents, consistently with observations, warmer than usual conditions are produced over India and Indochina, South Africa and Northeast America. Also, the cold area on the Southern US is correctly reproduced by the model. In the negative phase, shown in bottom panels, the most relevant patterns are correctly captured both over the oceans and over the continents.

4. PRELIMINARY RESULTS FROM THE NEW CMCC-SPS4 SEASONAL PREDICTION SYSTEM

This section is devoted to the preliminary assessment of the performances of the upcoming new CMCC-SPS4 operational system over the reforecast period. The analysis focuses on the two canonical start-dates of May and November and specifically on lead season one (JJA and DJF respectively).

The new operational system SPS4 has a nominal full ensemble size, in hindcast mode, of 30 members and the hindcast set covers a reference 30-year period, ranging from 1993 to 2022. At the moment of writing, only 13 ensemble members have been

produced. Moreover, the reference period is still incomplete and only years 1993-2003 for the November start-date and 1993-2002 for May have been covered by the reforecasts. Due to the very short period run and the small size of the ensemble available, the results are presented with the caveat that they should be considered very preliminary to evaluate the ability of the system of correctly reproducing the patterns and variability of the observed seasonal climate.

Nevertheless, the following results will show how the CMCC SPS4 system, is capable to represent the main features of the observed climate system, in terms of mean climate, seasonal variability and teleconnection patterns. The last point will be illustrated making use of the two indices presented in section 4, where they were applied to CMCC-CM3 (also referred to as CMCC-SPS4-CLIM). The system performance will be evaluated in terms of bias and anomaly correlation coefficients.

4.1. BIAS

Bias gives a measure of the systematic error of the model, expressing the difference between model and observed climatology. Biases are shown for the two main seasons: DJF (as lead season 1 of November start-dates) and JJA (as lead season 1 of May start-dates).

The November and May start date biases of t2m and Total Precipitation are shown in Figure 14. The patterns are very similar between seasonal prediction mode and constant forcing climate set-ups (compare with Figures 3 and 5). For November start date t2m, (top left panel), the cold bias over Northern America and Eurasian continent is intensified in the reduced ensemble hindcast seasonal system with respect to the model in climatological set-up (left upper panel of Figure 3). The warm bias over the North west Atlantic, instead, almost disappears. The precipitation field for the boreal winter (Figure

14 bottom left panel) shows, consistently with the left upper panel of Figure 5, dry regions along Alaska, the northern coasts of the Mediterranean basin, central Africa and the Maritime Continent. The main differences between the two model set-up biases are in the reduction of the very dry bias over South America in the CMCC-SPS4 and in the intensification of the wet bias over Australia.

Figure 14, right panels, shows the CMCC-SPS4 bias for May start-date and lead season 1, namely JJA. Similar considerations as for the DJF season apply: compared to the mean JJA season of the CMCC-SPS4-CLIM (shown in Figure 3), the t2m summer season bias of the CMCC-SPS4 exhibits common features. The most relevant features of Figure 14, top right panel, are the strong positive biases on the summer hemisphere land regions, the pattern over Equatorial oceans and the warm bias over Greenland. On the other hand, the two JJA climates (CLIM and Seasonal prediction mode) remarkably differ over the Southern Oceans and over Northern Siberia and Canada, where biases exhibit opposite signs. The bottom right panel of Figure 14 shows the precipitation bias of JJA, lead season 1 of May start-dates. Also in this case, the main patterns are very similar to the ones characterizing the climate set-up (Figure 5, left lower panel), with a strong dry bias over India and surrounding marine regions and dry biases over Europe, central USA and off the coasts of Alaska. On the other hand, the positive bias on the Pacific Tropical ocean is almost everywhere reduced, as it is the positive dry tongue on the Equatorial belt.

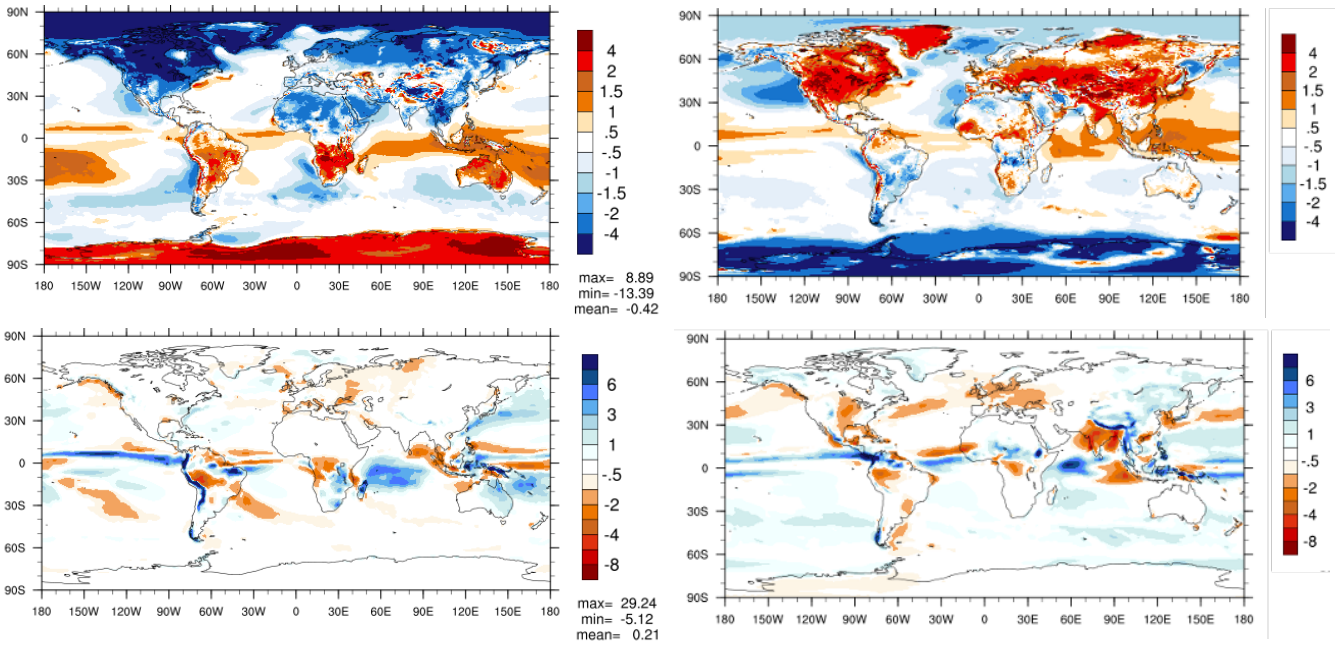

Figure 14. Lead season 1 bias with respect to observations (ERA5) for November start-date (left) and for May start-date (right). Top Panels show t2m bias (Celsius degrees), bottom panels show bias for Total Precipitation (mm, observations from GPCP). Analyzed period: 1993-2003. Ensemble size: 13 members.

4.2. ANOMALY CORRELATION COEFFICIENTS

The anomaly correlation coefficient is an index capturing the similarities in the patterns of the departures (anomalies) of the observed and forecast variables from the respective climatological means. In this report, the ACC is computed for the two analyzed start-dates of May and November and for the t2m and Total Precipitation fields.

We recall that the results shown are very preliminary, computed over a short reference period and with a reduced ensemble size. The very noisy patterns presented in the following figures are a consequence of these two factors. Nevertheless, the indices prove that the system is able to capture the main observed variabilities.

To allow for a comparison with the performances of the current operational seasonal forecast system, the ACC has been recomputed also for the CMCC-SPS3.5 hindcasts, subsampling both the ensemble size and the reforecast period in order to have the same number of members and years involved (13 members and 11 years for November/10 for May).

Figure 15 illustrates the t2m (top panels) and precipitation (bottom panels) ACC for the DJF season, lead season 1, November start-date. The CMCC-SPS4 skill score, computed on the preliminary results of the hindcasts (left panels), is contrasted against the ACC computed from the currently operational CMCC-SPS3.5 (right panels). The main features of the t2m maps are very similar, with very high skill over Tropical Oceans and South America, a and rather poor performance over the other continental areas. The increase in the global value of the ACC is mainly the consequence of the improved performance over the Tropical Atlantic Ocean.

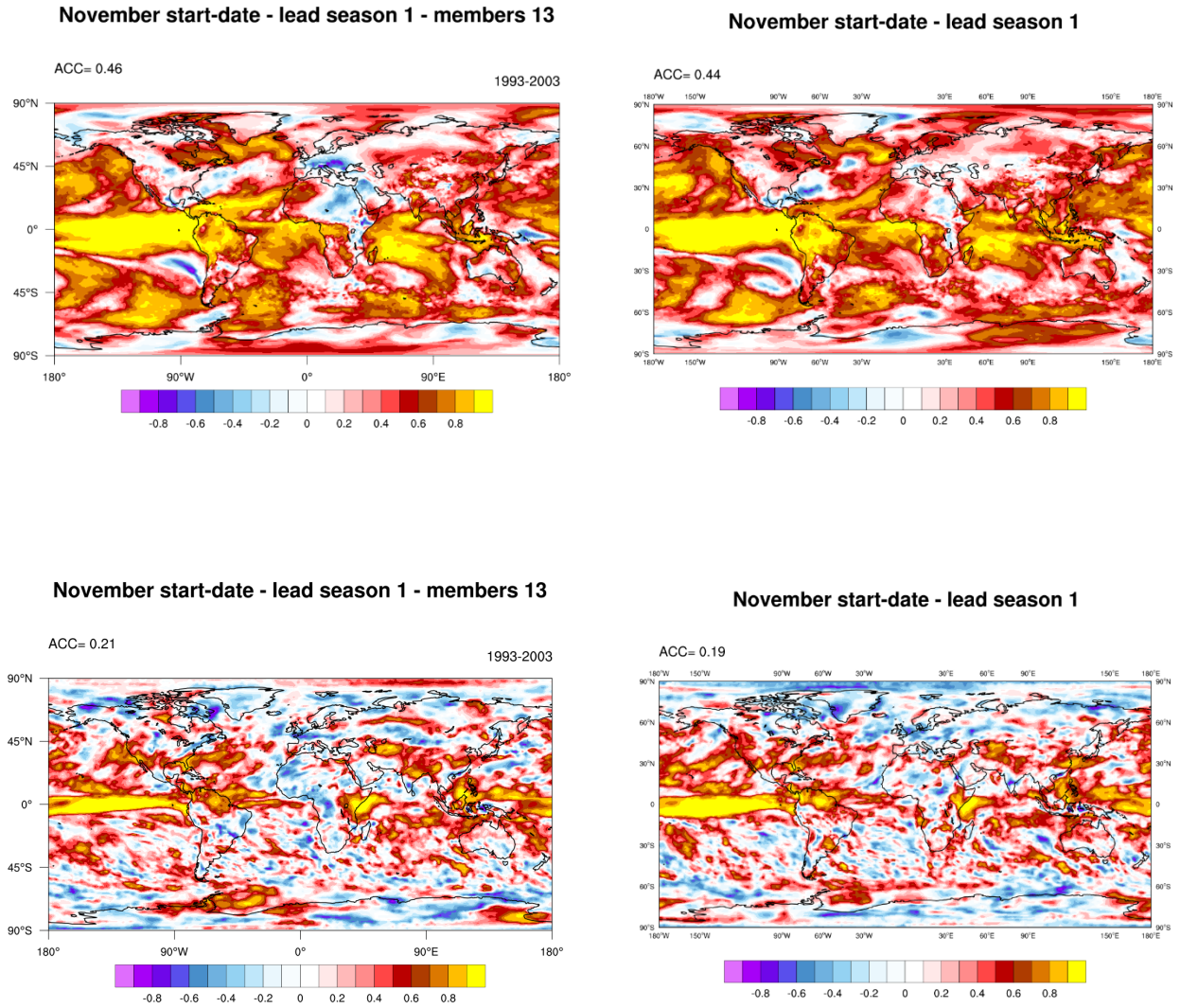

Figure 15. Anomaly correlation coefficients computed for t2m field (top) and Precipitation (bottom), November start-dates, lead season 1 (DJF). Left panels show CMCC-SPS4 13-member ensemble mean, reference period 1993-2003; right panels CMCC-SPS3.5, with reduced ensemble size and reference period to make it comparable to the new system. Observations come from ERA5 (GPCP for precipitation).

Also for Total Precipitation (bottom panels), the main features of the skill score are common to the two panels: very high performance over tropical Pacific and sparse regions of good performance, over central Asia and central North America. Again, the global ACC value is slightly higher in the new CMCC-SPS4 system (left panel), yet the figures are quite low.

Similar to Figure 15, Figure 16 illustrates the same ACCs, but for the JJA season, lead season 1, May start-date. The two CMCC-SPSs again share the main patterns for t2m (top), with an increased performance over Tropical Atlantic for CMCC-SPS4, which explains the slight gain in the score at a global scale also for this season. For precipitation (bottom panels), again the patterns are very similar, especially over the Tropical belt. Some regions seem to lose skill (e.g. India) while others slightly gain in performance (North Atlantic). We emphasize that, despite the quite large dry bias in precipitation over India, on JJA lead season 1 issued in May (Figure 14 panel bottom right), the ACC on the same region is not compromised, implying that the model is still capable of representing the observed seasonal variability.

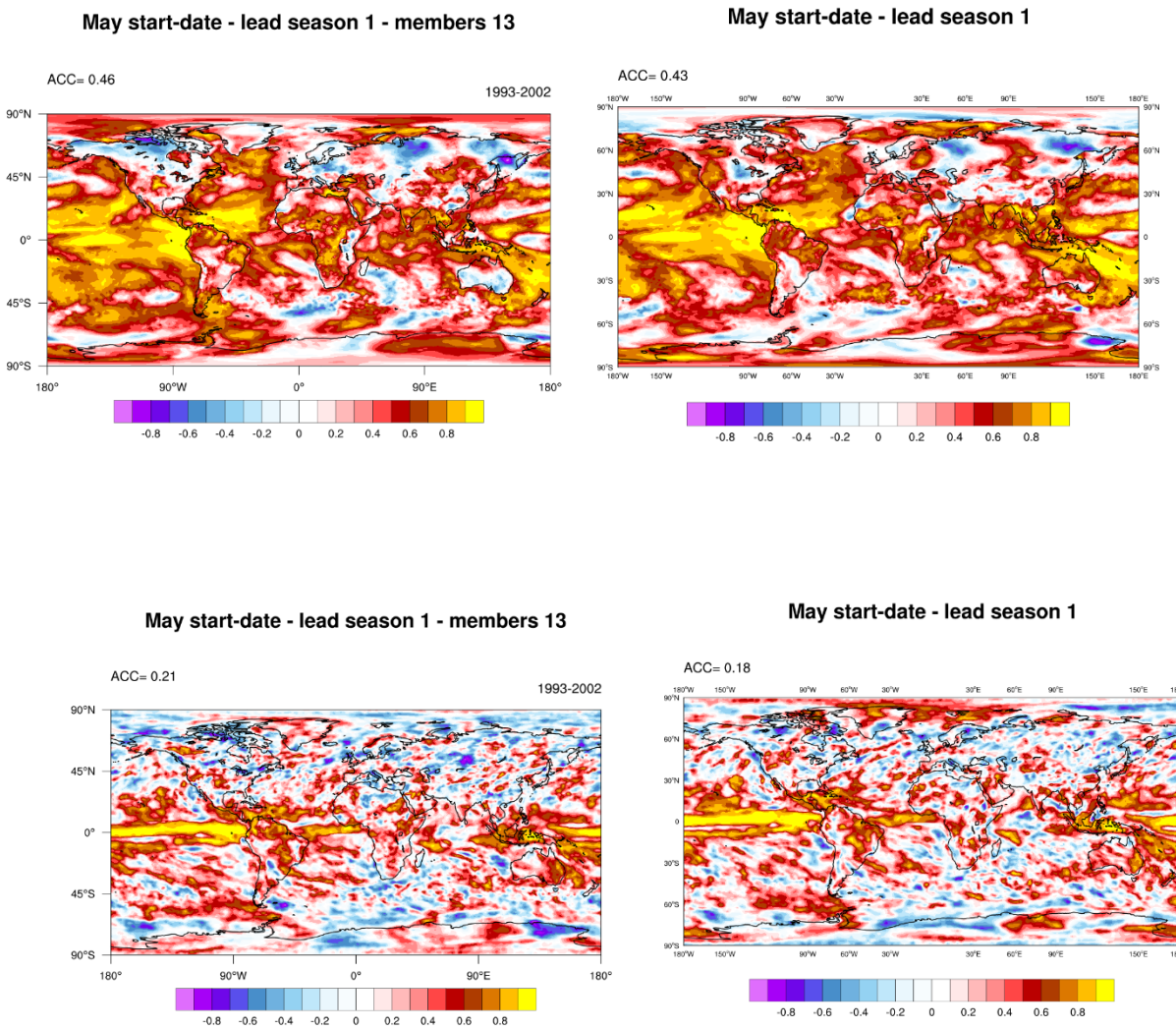

Figure 16. t2m (top panels) and precipitation (bottom panels) ACC for May start-dates, lead season 1 (JJA). Reference period here is 1993-2002. Left panel CMCC-SPS4, right panel CMCC-SPS3.5. Observations come from ERA5 (GPCP for precipitation).

4.3. CLIMATE VARIABILITY INDICES

This section is devoted to the preliminary investigation of the CMCC-SPS4 system capability of reproducing some features of the internal variability of the climate system. The same teleconnection indices analyzed in section 4, namely NAO and Nino3.4, are computed in the seasonal forecast set-up and discussed in the present subsection. The composites on their two phases are computed (similarly to what done in section 4.3.1 and 4.3.2) and compared to observations over the period 1993-2016. The choice of comparing different periods has been made following Molteni and Brookshaw (2023), in order to decrease the 'noise' generated by the 'single realization per year' in the observations and, as a consequence, to reduce the differences with respect to the smoother ensemble composites. For the sake of comparison, the same observation composites presented in section 4.3 are plotted again with model ones.

4.3.1. NAO COMPUTED FROM SEASONAL FORECAST RUNS

The NAO index is computed, following the definition of Li and Wang 2003, both for the observations, provided by ERA5, over the hindcast period 1993-2003 covered so far, and for the CMCC-SPS4 forecasts, presented in terms of monthly mean ensemble means (Figure 17, observations in red and model monthly mean ensemble means in black). With respect to Figure 8, the CMCC-SPS4 results show a better agreement with the inception of the NAO phases, in connection to the interannual variability forcings correctly represented by the model run in seasonal-prediction mode.

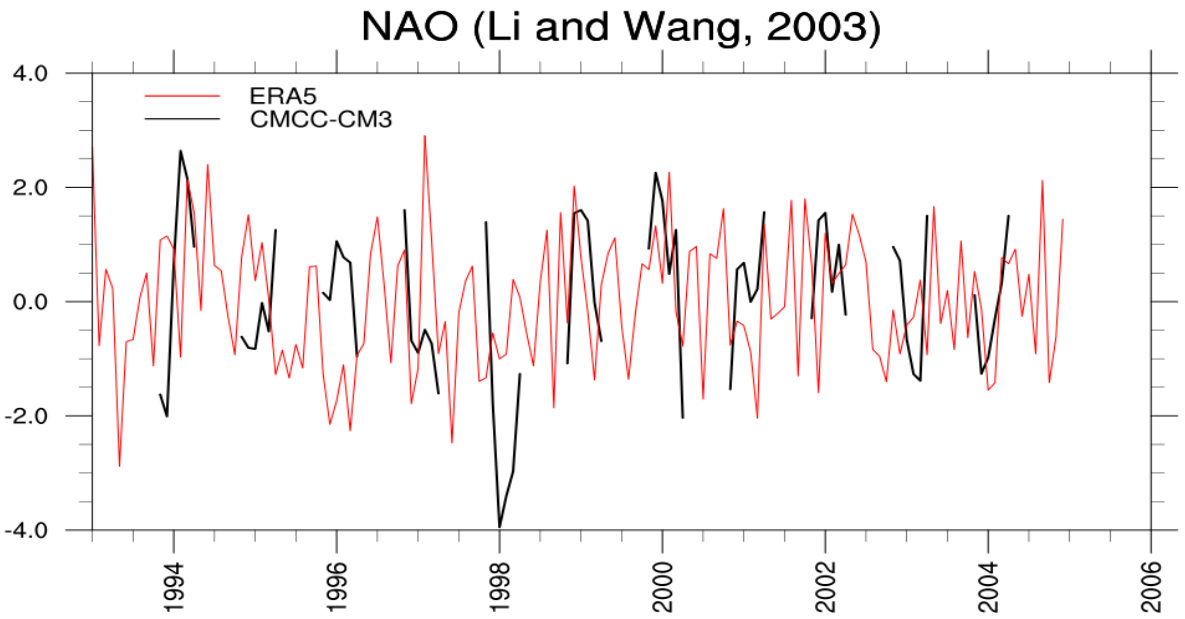

Figure 17: monthly timeseries of the monthly (a-dimensional) NAO index (Li and Wang, 2003). The black curves represent the ensemble means of the available 13-member November 6-month-long hindcasts; the red curve is the observations from ERA5. Data from the reference period 1993-2003, covered by the November hindcasts at the time of writing.

Figure 18 shows the composites of Total Precipitation anomalies of the boreal winter NAO, computed from November start-date lead season 1. Model results are shown on the left, while those computed from the GPCP are on the right; the positive phase is displayed on the top and the negative one on the bottom. In the NAO positive phase, the model reproduces the main relevant features of the observed teleconnection pattern, notably the dry anomalies on the Mediterranean Basin and Southern Europe, along with

the wetter than usual conditions over the northern European countries. Going into detail, the model composite exhibits a more defined zonal structure with respect to the observations, which show a more complex pattern; moreover, the wet regions in the model composite are shifted northward with respect to the GCPC. The negative phase shows a pattern which is the very symmetric of the positive one. Besides the marked zonal feature of the model, also in this case (with opposite sign), the dry regions are displaced farther north with respect to the observations. Nevertheless, the most relevant signal of wetter than usual conditions over Mediterranean Sea is correctly captured and reproduced by the model (even if more spread over the Mediterranean Basin than in the real world).

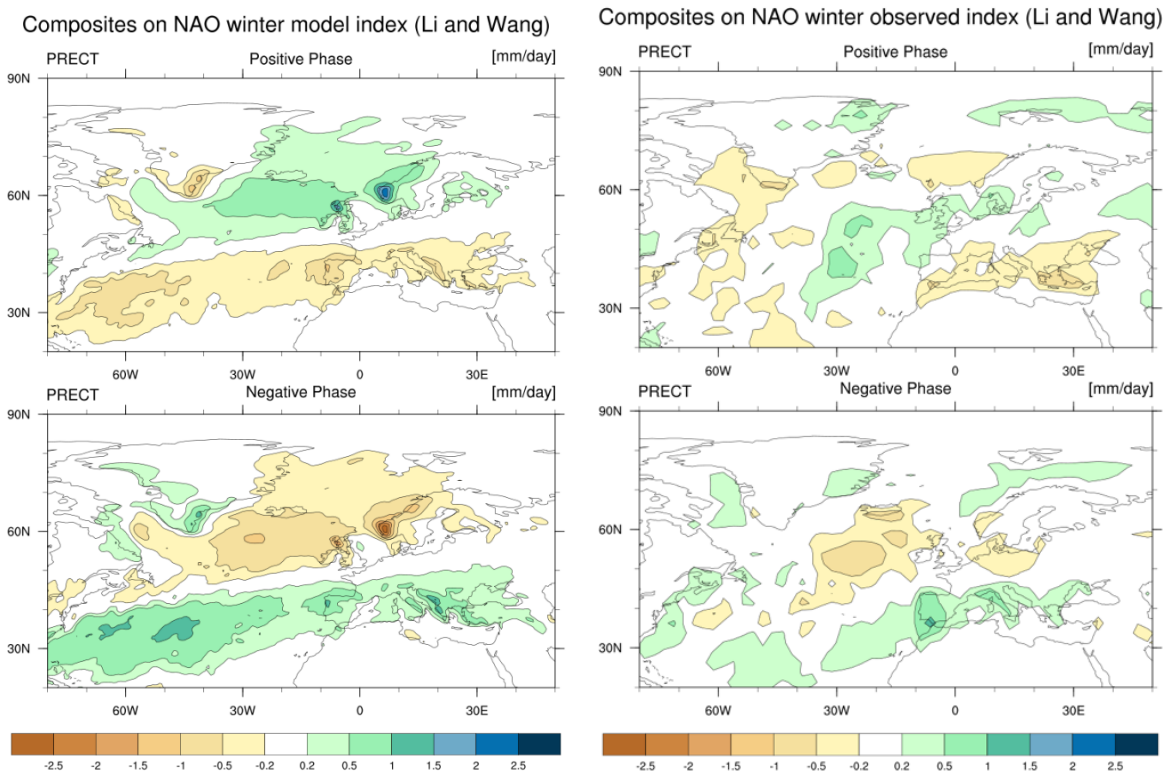

Figure 18: Boreal winter (DJF) composites of precipitation for NAO. Left panels show model results and right ones composites based on GPCP; positive phases are displayed on the upper panels while negative phases on the lower ones.

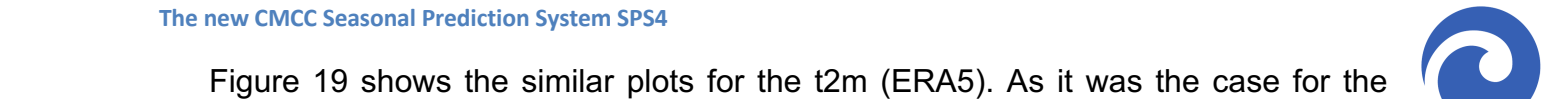

Figure 19 shows the similar plots for the t2m (ERA5). As it was the case for the composites based on precipitation, the most relevant feature is the almost perfect symmetry between the positive and negative phase in the model world. Real world patterns are more complex and less symmetric. Examining the positive phase (top panels), the signal of higher than normal t2m over continental Europe (top right panel) is correctly reproduced by the model (top left), though with stronger intensity. In the negative phase (bottom panels), consistently with what observed for precipitation, a northward shift of negative anomaly centered on central Europe is evident in the model. The anomalies in the model are overall stronger than in the observations.

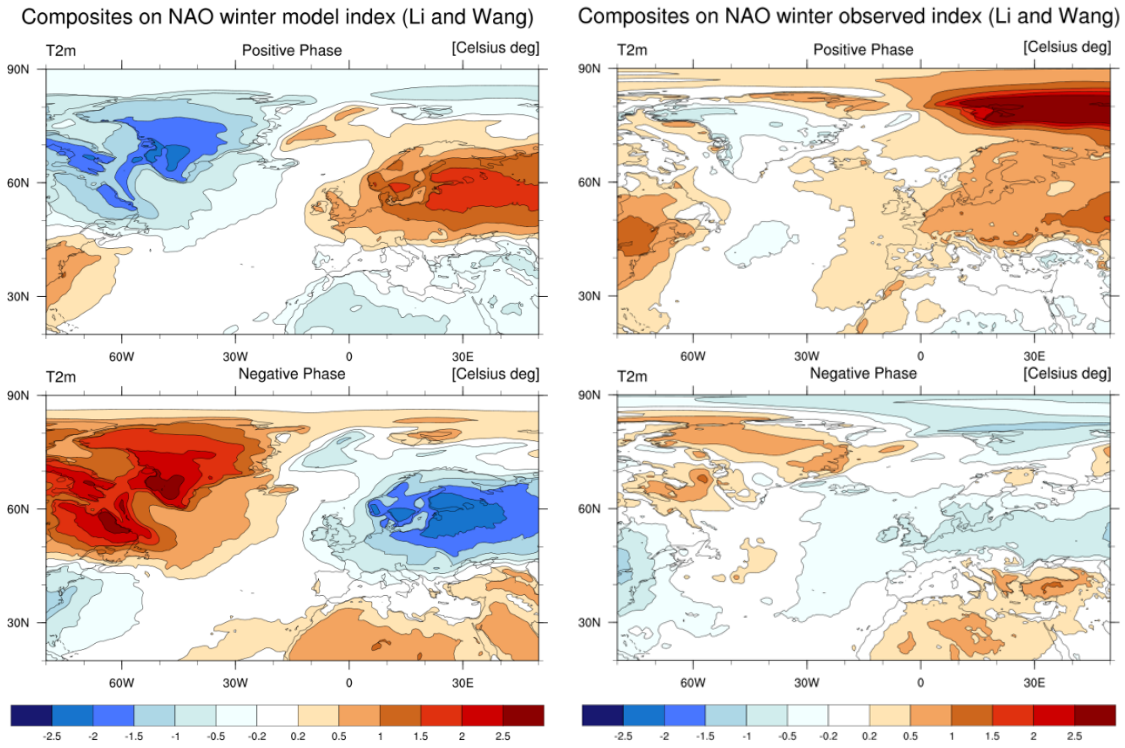

Figure 19: Boreal winter (DJF) composites of 2m-temperature for NAO. Left panels show model results and right ones composites based on ERA5 re-analyses; positive phase are displayed on the upper panels while negative phase on the lower ones.

4.3.2. ENSO COMPUTED FROM SEASONAL FORECAST RUNS

The CMCC-SPS4 ability to reproduce the climate variability associated to ENSO is analyzed in terms of the Nino3.4 index, similarly to what was done for the CMCC-SPS4-CLIM in section 4.

Figure 20 shows the timeseries of the SST Equatorial Pacific in red, over the available hindcast period 1993-2002, and the CMCC-SPS4 6-month 13-member ensemble means in black. The agreement between model results and observations is almost everywhere remarkable, confirming the capability of the new CMCC-SPS4 system to realistically represent the most important source of global predictability in the framework of seasonal forecasts.

Similarly to what presented for NAO, the DJF composites of precipitation and t2m over the two phases of Nino3.4 CMCC-SPS4 November start-dates are analyzed and contrasted against the observations (GPCP for precipitation and ERA5 for t2m), over the hindcast reference period 1993-2016.

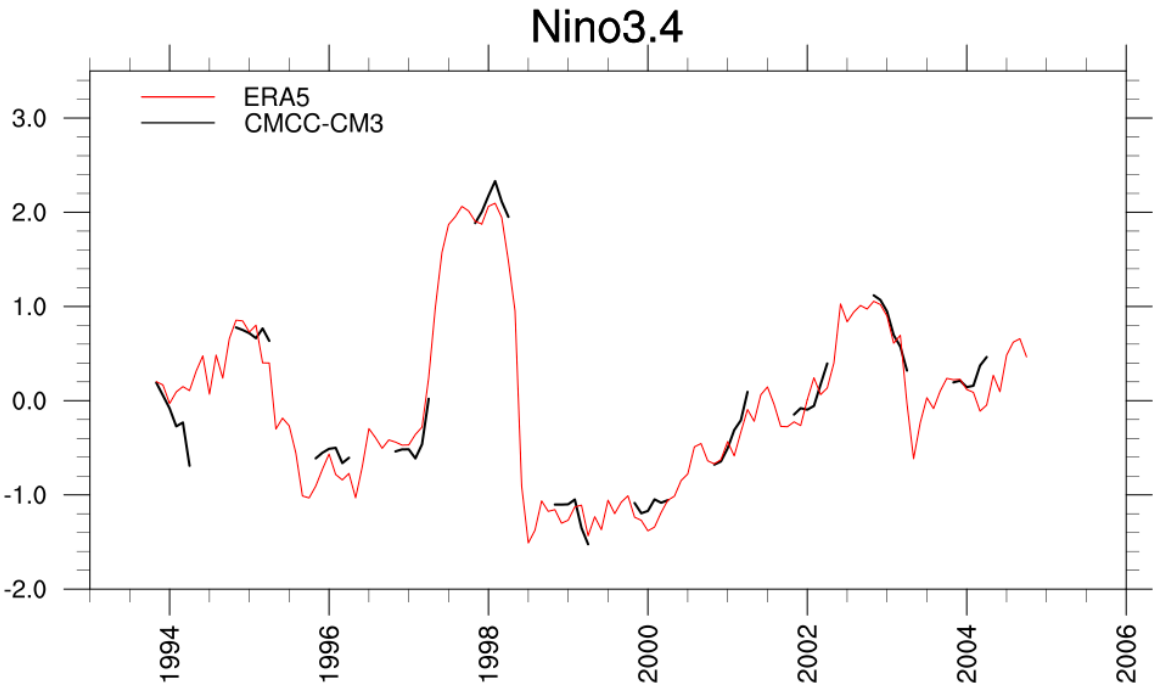

Figure 20: Monthly timeseries of Nino3.4 index. The black curves are the ensemble mean of the available 13-member November 6-month-long hindcasts, while the red one represents the observations from ERA5. The period 1993-2003 shown is the reference period covered by the November hindcast at the moment of the report drafting.

Figure 21 compares the composites computed from precipitation field, with model results on the left panels and observations on the right. The teleconnection pattern of the observed positive phase (top right panel) is very well captured over the Southern Hemisphere and the Tropical Belt (top left). Also in the negative phase (bottom panels), the model exhibits a fairly good correspondence with the observations. Though the extent of the anomalies is overall largely underestimated, the main features of the teleconnection are correctly represented.

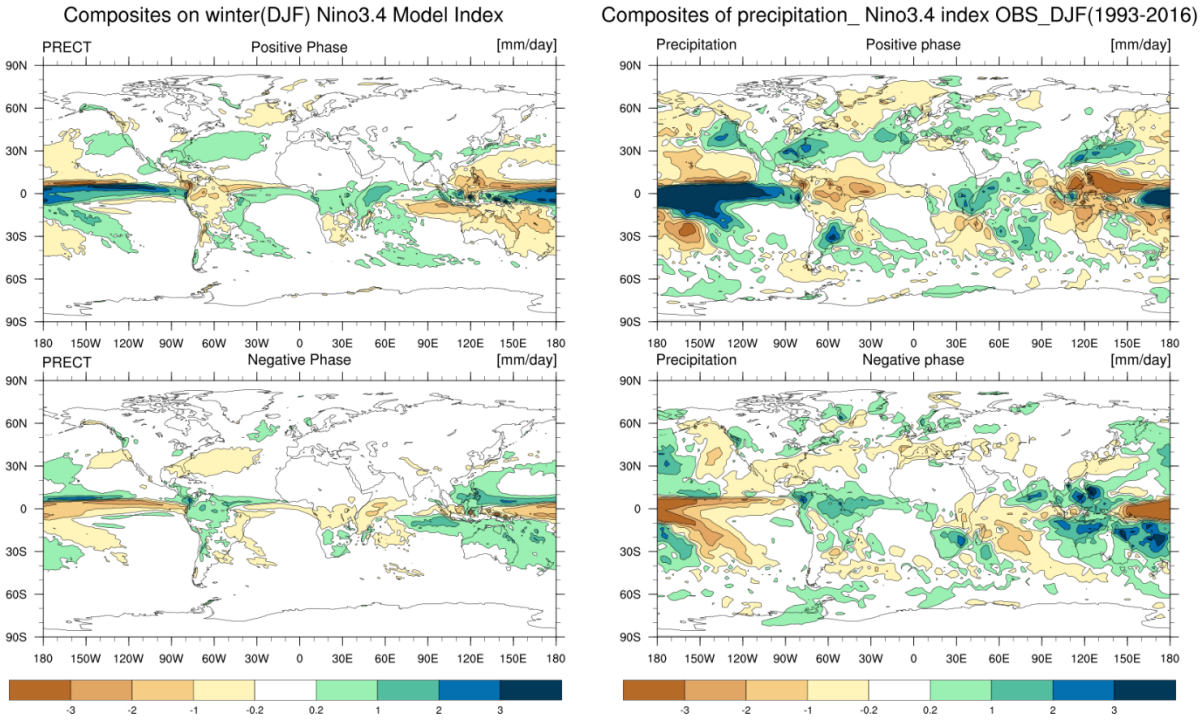

Figure 21: Boreal winter (DJF) composites of Total Precipitation in the boreal winter Nino3.4. Upper panels show the positive phase and lower ones negative one. Only available reforecasts used (13 members, over 1993-2003). Left panels model, right panels observations (GPCP).

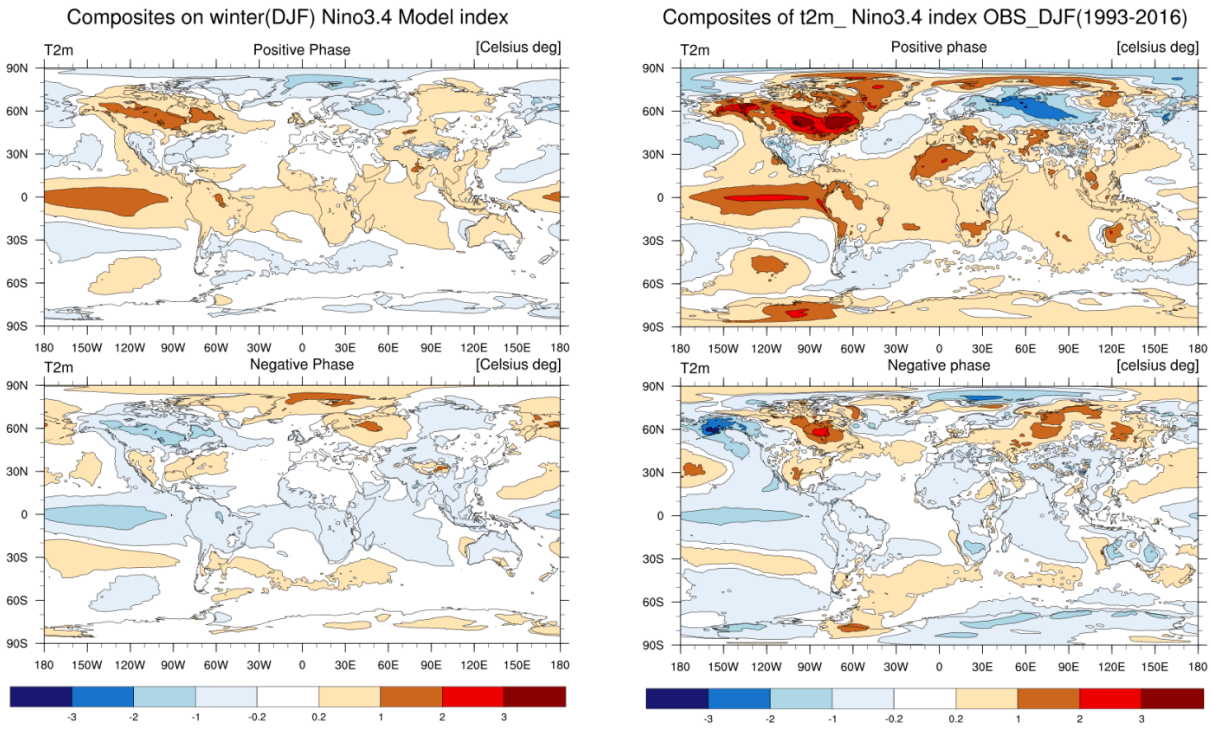

Figure 22: Same as Figure 21 but for t2m. Observations are ERA5.

Figure 22 presents the composites from t2m field. As in the previous Figures, top panels show the positive phase, while bottom ones the negative. In the positive phase, the model (top left) captures some relevant features of the Nino teleconnection, such as the positive anomalies over North-western Australia, the Maritime continent, India and over South Africa. The anomaly over Alaska is fairly well reproduced, even if with weaker intensity. Concerning the negative phase (bottom panels), a good correspondence between model and observations is observable overall in the Southern Hemisphere, where the fingerprints of the teleconnection are indeed stronger.

Overall, the system proves to adequately capture the main characteristics of the most important source of seasonal predictability.

5. CONCLUSIONS

The newly developed Seasonal Prediction System CMCC-SPS4 has been presented and described in its main constitutive characteristics.

Section 2 has been devoted to the description of the underlying earth system model CMCC-CM3. The performance of the new model has been evaluated in terms of a present-climate (2000 perpetual periodic forcing 30-year run) in Section 3 and preliminary results of its skills in seasonal prediction mode (CMCC-SPS4) have been illustrated in Section 4.

The new model exhibits some relevant strengths with respect to the old one (especially in the overall temperature biases and in the representation of the QBO). The SPS4 configuration at present does not show any shortcomings with respect to the current operational system. The ensemble size and the reforecast period available at the moment of writing this report are too small and too short to draw robust conclusions. Nevertheless, the comparison with observations exhibits satisfactory preliminary results both in terms of variability and intensity of the main predictability indices and the associated climate regimes. Other diagnostics will be applied in the future diagnostics, to further investigate the improvements that the system should have derived from a much-improved simulation of the Stratosphere.

6. ACKNOWLEDGEMENTS

The Precipitation – GPCP Monthly CDR used in this document was acquired from the NOAA National Centers for Environmental Information (NCEI; formerly NCDC) (https://www.ncei.noaa.gov). This CDR was developed by Robert Adler, Mathew Sapiano, JianJian Wang of the University of Maryland College Park. The re-analysis products used in this report were provided by the Copernicus Climate Change Service (2023): ERA5 hourly data on single levels from 1940 to present. Copernicus Climate Change Service (C3S) Climate Data Store (CDS), DOI: 10.24381/cds.adbb2d47 (Accessed on 07-MAR-2023)

BIBLIOGRAPHY

Adler, R.F., G.J. Huffman, A. Chang, R. Ferraro, P. Xie, J. Janowiak, B. Rudolf, U. Schneider, S. Curtis, D. Bolvin, A. Gruber, J. Susskind, P. Arkin, E. Nelkin, 2003. "The Version 2 Global Precipitation Climatology Project (GPCP) Monthly Precipitation Analysis (1979-Present)," J. Hydrometeor., vol. 4, pp. 1147-1167.

Anderson, E.A. 1976. A point energy and mass balance model of a snow cover. NOAA Technical Report NWS 19, Office of Hydrology, National Weather Service, Silver Spring, MD.

Beljaars, A. C. M., Brown, A. R., & Wood, N. (2004). A new parameterization of turbulent orographic form drag. Quarterly Journal of the Royal Meteorological Society, 130, 1327–1347. https://doi.org/10.1256/qj.03.73

Brodeau, L., B. Barnier, S. K. Gulev, and C. Woods, 2017: Climatologically Significant Effects of Some Approximations in the Bulk Parameterizations of Turbulent Air–Sea Fluxes. J. Phys. Oceanogr., 47, 5–28, https://doi.org/10.1175/JPO-D-16-0169.1.

Cherchi, A., Fogli, P. G., Lovato, T., Peano, D., Iovino, D., Gualdi, S., et al. (2019). Global mean climate and main patterns of variability in the CMCC-CM2 coupled model. Journal of Advances in Modeling Earth Systems, 11, 185– 209. https://doi.org/10.1029/2018MS001369

Craig, C., Bacmeister, J., Callaghan, P., Eaton, B., Gettelman, A., Goldhaber, S. N., et al. (2021). CAM6.3 user's guide (Technical Report). NCAR/TN-571+EDD. https://doi.org/10.5065/Z953-ZC9

Danabasoglu, G., Lamarque, J.-F., Bacmeister, J., Bailey, D. A., DuVivier, A. K., Edwards, J., et al. (2020). The Community Earth System Model Version 2 (CESM2). Journal of Advances in Modeling Earth Systems, 12, e2019MS001916. https://doi.org/ 10.1029/2019MS001916

Darcy, H. (1857). Recherches expérimentales relatives au mouvement de l'eau dans les tuyaux (Vol. 1). Mallet-Bachelier

Flanner, M.G., and Zender, C.S. 2006. Linking snowpack microphysics and albedo evolution. J. Geophys. Res. 111:D12208. DOI:10.1029/2005JD006834.

Gettelman, A., & Morrison, H. (2015). Advanced two-moment bulk microphysics for global models. Part I: Off-line tests and comparison with other schemes. Journal of Climate, 28, 1268–1287. https://doi.org/10.1175/JCLI-D-14-00102.1

Golaz, J.-C., Larson, V. E., & Cotton, W. R. (2002). A PDF-based model for boundary layer clouds. Part I: Method and model description. Journal of the Atmospheric Sciences, 59, 3540–3551.

Graham, S.T., Famiglietti, J.S., and Maidment, D.R. 1999. Five-minute, 1/2o, and 1o data sets of continental watersheds and river networks for use in regional and global hydrologic and climate system modeling studies. Water Resour. Res. 35:583-587.

Hibler, W.D. (1979) A dynamic thermodynamic sea ice model. J. Phys. Oceanogr., 9:817–846. URL: http://dx.doi. org/10.1175/1520-0485(1979)009\T1\textless{}0815:ADTSIM\T1\textgreater{}2.0.CO;2.

Hunke, E. C., and J. K. Dukowicz, 1997: An Elastic–Viscous–Plastic Model for Sea Ice Dynamics. J. Phys. Oceanogr., 27, 1849–1867, https://doi.org/10.1175/1520-0485(1997)027<1849:AEVPMF>2.0.CO;2.

Hunke, E., Allard, R., Bailey, D. A., Blain, P., Craig, A., Damsgaard, A., DuVivier, A., Grumbine, R., Hebert, D., Holland, M., Jeffery, N., Lemieux, J.-F., Rasmussen, T., Turner, M., Ribergaard, M., Roberts, A., & Winton, M.. (2018). CICE-Consortium/CICE: CICE version 6.0.0 (CICE6.0.0). Zenodo. https://doi.org/10.5281/zenodo.1900639

Iacono, M. J., Delamere, J. S., Mlawer, E. J., Shephard, M. W., Clough, S. A., & Collins, W. D. (2008). Radiative forcing by long-lived greenhouse gases: Calculations with the AER radiative transfer models. Journal of Geophysical Research, 113, D13103. https://doi.org/ 10.1029/2008JD009944

Koven, C. D., Riley, W. J., Subin, Z. M., Yang, J. Y., Torn, M. S., Collins, W. D., et al. (2013). The effect of vertically resolved soil biogeochemistry and alternate soil C and N models on C dynamics of CLM4. Biogeosciencies, 10(11), 7109–7131 https://doi.org/10.5194/bg-10-7109-2013.

Larson, V. E., (2017). CLUBB-SILHS: A parameterization of subgrid variability in the atmosphere. arXiv:1711.03675v2 [physics.ao-ph].

Lawrence, D. M., Fisher, R. A., Koven, C. D., Oleson, K. W., Swenson, S. C., Bonan, G., et al. (2019). The Community Land Model version 5: Description of new features, benchmarking, and impact of forcing uncertainty. Journal of Advances in Modeling Earth Systems, 11, 4245–4287. https://doi.org/10.1029/2018MS001583

Li J, Wang J (2003) A new North Atlantic Oscillation index and its variability. Adv Atmos Sci 20:661–676. doi:10.1007/BF02690792

Lin, S. J., & Rood, R. B. (1997). An explicit Flux-Form Semi-Lagrangian shallow water model on the sphere. Quarterly Journal of the Royal Meteorological Society, 123, 2477–2498.

Liu, X., Ma, P. L., Wang, H., Tilmes, S., Singh, B., Easter, R. C., et al. (2016). Description and evaluation of a new four-mode version of the Modal Aerosol Module (MAM4) within Version 5.3 of the Community Atmosphere Model. Geoscientific Model Development, 9, 505–522. https://doi.org/10.5194/gmd-9-505-2016

Locarnini, R. A., A. V. Mishonov, O. K. Baranova, T. P. Boyer, M. M. Zweng, H. E. Garcia, J. R. Reagan, D. Seidov, K. Weathers, C. R. Paver, and I. Smolyar, 2018. World Ocean Atlas 2018, Volume 1: Temperature. A. Mishonov Technical Ed.; NOAA Atlas NESDIS 81, 52pp.

Madec, G., & Imbard, M. (1996). A global ocean mesh to overcome the North Pole singularity. Climate Dynamics, 12, 381–388.

Madec, G., Bourdallé-Badie, R., Chanut, J., Clementi, E., Coward, A., Ethé, C., Iovino, D., Lea, D., Lévy, C., Lovato, T., Martin, N., Masson, S., Mocavero, S., Rousset, C., Storkey, D., Müeller, S., Nurser, G., Bell, M., Samson, G., Mathiot, P., Mele, F., Moulin, A. (2022). NEMO ocean engine. Scientific Notes of Climate Modelling Center, 27 - ISSN 1288-1619, Institut Pierre-Simon Laplace (IPSL), doi:10.5281/zenodo.1464816.

Materia, S., Peano, D., Lovato, T., Benassi, M., Gualdi, S., Alessandri, A., Navarra, A. (in prep). An enhanced river routing scheme for the closure of global water budget.

Molteni, F., Brookshaw, A. Early- and late-winter ENSO teleconnections to the Euro-Atlantic region in state-of-the-art seasonal forecasting systems. Clim Dyn 61, 2673–2692 (2023). https://doi.org/10.1007/s00382-023-06698-7

Scinocca, J., & Mcfarlane, N. (2000). The parametrization of drag induced by stratified flow over anisotropic orography. Quarterly Journal of the Royal Meteorological Society, 126, 2353–2394. https://doi.org/10.1256/smsqj.56801

van Kampenhout, L., J.T.M. Lenaerts, W.H. Lipscomb, W.J. Sacks, D.M. Lawrence, A.G. Slater, and M.R. van den Broeke, 2017. Improving the Representation of Polar Snow and Firn in the Community Earth System Model. Journal of Advances in Modeling Earth Systems 9, no. 7: 2583–2600. https://doi.org/10.1002/2017MS000988.

Yin L., R. Fu, E. Shevliakova and E. Dickinson, 2012: How well can CMIP5 simulate precipitation and its controlling processes over tropical South America?. Climate Dynamics 41: 3127-3143.

Weisbach, J. L. (1845). Lehrbuch der ingenieur-und maschinen-mechanik: Theoretische mechanik (Vol. 1). Druck und Verlag von Friedrich Vieweg und Sohn.

Zweng, M. M., J. R. Reagan, D. Seidov, T. P. Boyer, R. A. Locarnini, H. E. Garcia, A. V. Mishonov, O. K. Baranova, K. Weathers, C. R. Paver, and I. Smolyar, 2018. World Ocean Atlas 2018, Volume 2: Salinity. A. Mishonov Technical Ed.; NOAA Atlas NESDIS 82, 50pp.